Mechatronics 76 (2021) 102543

Contents lists available at ScienceDirect

Mechatronics

journal homepage: www.elsevier.com/locate/mechatronics

PID-type sliding mode-based adaptive motion control of a 2-DOF piezoelectric ultrasonic motor driven stage

Min Ming [a,b], Wenyu Liang [b,c], Zhao Feng [a], Jie Ling [a], Abdullah Al Mamun [b], Xiaohui Xiao [a,*]

[a] School of Power and Mechanical Engineering, Wuhan University, Wuhan 430072, China
[b] Department of Electrical and Computer Engineering, National University of Singapore, 117576, Singapore
[c] Institute for Infocomm Research, Agency for Science, Technology and Research, 138632, Singapore

ARTICLE INFO

Keywords:
Adaptive control
Ultrasonic motor
Multi-DOF stage
Unilateral coupling

ABSTRACT

This paper presents a new scheme of adaptive sliding mode control (ASMC) for a piezoelectric ultrasonic motor driven X–Y stage to meet the demand of precision motion tracking while addressing the problems of unknown nonlinear friction and model uncertainties. The system model with Coulomb friction and unilateral coupling effect is first investigated. Then the controller is designed with adaptive laws synthesized to obtain the unknown model parameters for handling parametric uncertainties and offsetting friction force. The robust control term acts as a high gain feedback control to make the output track the desired trajectory fast for guaranteed robust performance. Based on a PID-type sliding mode, the control scheme has a simple structure to be implemented and the control parameters can be easily tuned. Theoretical stability analysis of the proposed novel ASMC is accomplished using a Lyapunov framework. Furthermore, the proposed control scheme is applied to an X–Y stage and the results prove that the proposed control method is effective in achieving excellent tracking performance.

1. Introduction

There are many applications nowadays that require precision motion control, *e.g.*, atomic force microscopy [1], nanopositioner [2,3] microgrippper [4], robot-assisted surgeries, medical devices [5–7], and so on. In these applications, piezoelectric actuators are widely used because of their ultra-high resolution and fast response, which make them achieve high-precision and high-speed motion. Piezoelectric ultrasonic motor (PUM) is a type of direct-drive motor that is powered by a piezoelectric component [8]. Due to the merits of the piezoelectric component, the PUM has a compact size and can achieve high-speed and high-precision motion. However, designing a controller that can achieve high tracking performance is still a challenge to these motion systems due to nonlinear behavior of actuators, parametric uncertainties, and unmodeled disturbances. For a PUM, the nonlinear friction force is the main factor affecting tracking performance. Furthermore, a 2-DOF stage, consisting of two orthogonal ultrasonic motors, gives rise to problems due to coupling if (a) there is any deviation from angles at the time of installation of the stage, and (b) there is any misalignment between the center of the load and the center of the stage [9].

Many robust controllers have been proposed in the published literature to address the issues of uncertainties and disturbances, *e.g.*, disturbance observer-based control [10–13], sliding mode control (SMC) [14–17], adaptive robust control (ARC) [18], intelligent control [8], neural network-based (NN-based) control [19,20], and so on. These works used different devices to underscore the effectiveness of their methods. In observer-based controllers, nonlinearities, model uncertainties, and disturbances are treated as a lump disturbance to a nominal linear model. A disturbance observer is often adopted to observe and compensate the lump disturbance and feedback control is used to achieve the object of desired tracking performance. SMC is a practical variable structure control to cope with all bounded disturbances and achieve asymptotic tracking performance. An extended state observer (ESO) combined with SMC is an effective strategy [21]. In [11], disturbance compensation via ESO is developed and a model-based second-order sliding function is designed. It also concludes that the integral sliding mode control can improve the tracking performance by introducing the integral term of tracking error [13]. However, ESO is limited by its bandwidth and, therefore, can only perform well for low-frequency reference trajectories. It is reported in [22] that a static friction model can predict the friction phenomenon with almost the same performance as using a dynamic friction model. The static friction model is identified and used for feedforward compensation in [22,23]. Although many friction models are proposed in [24], the traditional compensation schemes using the static friction model may not be valid in some

* Corresponding author.
E-mail address: xhxiao@whu.edu.cn (X. Xiao).

https://doi.org/10.1016/j.mechatronics.2021.102543
Received 13 April 2020; Received in revised form 19 February 2021; Accepted 7 March 2021
Available online 13 April 2021

practical applications where the friction force is varying and uncertain. Therefore, unknown model uncertainties and friction force should be estimated and compensated in real-time to improve the control accuracy of SMC and achieve tracking faster desired trajectories.

Adaptive control is a good choice for improving tracking accuracy when model parameters to be estimated are unknown but constant. A robust controller that merges sliding-mode and adaptive schemes is proposed in [25], where the adaptive part is used to cope with unknown slow-time varying disturbances. ARC proposed in [26] is very suitable for a class of systems with unknown nonlinear model. It combines parametric adaptive law with deterministic robust control, namely high gain feedback control. The system model established in [26] consists of a dynamic part with Coulomb friction, and the unknown parameters are estimated using adaptive law. This control scheme has been successfully applied to many practical applications [18,27,28]. However, it is mentioned in [29] that ARC can only guarantee the tracking error convergences to a specified limit set because the feedback control gains cannot be set to infinity. The robust integral of the sign of error (RISE) controller developed in [30] can achieve asymptotic tracking performance when the disturbance is assumed to be second-order derivable and bounded [31]. A RISE-based adaptive controller (ARISE) is proposed in [29] for a hydraulic system. It is worth noting that for a second-order system, the essential difference between ARISE and ARC is that the high gain feedback control law in ARISE includes the integral terms of the error and the sign of the error. When the disturbance is small, the integral term of the sign of the error is negligible. It is also verified that introducing integral terms of error to the control law can improve the tracking performance in [13,32]. It should be noted that an integral sliding surface not only can reduce the steady-state error but also can provide faster response and more accurate trajectory tracking performance than the common PD-type sliding surface. To integrate the integral term, the PID-type sliding mode function has been adopted in [32–34].

Though the existing control strategies for systems with nonlinear friction and uncertainty show great improvements, the following two aspects can be further improved: (a) it is important to adopt active compensation to alleviate the nonlinearity and uncertainty so that the controller can achieve improved performance and be suitable for fast tracking, and (b) the asymptotic tracking performance can be obtained by integrating the benefits of the SMC and the advanced controller ARISE, which can be realized by using a PID-type sliding mode function. Therefore, this paper presents a novel adaptive sliding mode control (ASMC) by combining PID-type sliding surface-based SMC and adaptive control, which makes the proposed controller have advantages in terms of strong robustness and high tracking performance.

The main contributions of this paper can be summarized as follows. First, it is desirable that a controller is designed with a clear structure, is easy in tuning, and can achieve high tracking performance. There is no requirement to have a specific knowledge of the friction and cross effect. The adaptive control law is designed to estimate the model parameters and disturbance simultaneously. The adaptive control is designed to realize active compensation and relieve the chattering phenomenon. The PID-type sliding mode including the integral term with a simple structure can further improve the tracking performance. More precisely, the proposed controller (ASMC) consists of two terms: (1) a model compensation term related to the reference trajectory which is adjustable with estimating model parameters via adaptive technique, and (2) a feedback robust term. The stability of the proposed control scheme is proven in the Lyapunov framework. Finally, to demonstrate the effectiveness of the proposed controller in achieving high tracking performance, extensive comparative experiments are conducted on an ultrasonic-motor-driven 2-DOF stage.

The main content of this paper is organized as follows. The system description and control problem statement are introduced in Section 2. Section 3 gives the detailed steps of controller design and stability analysis, and the experimental setup is described in Section 4. Experiments and comparisons of the results are presented and discussed in Section 5. Some conclusions are summarized in Section 6.

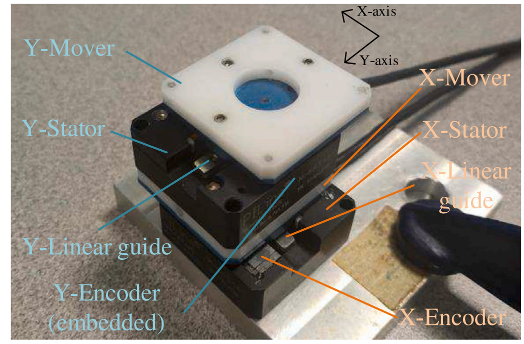

Fig. 1. Piezoelectric ultrasonic motor driven 2-DOF stage.

2. System description and control problem statement

2.1. 2-DOF system

The 2-DOF piezoelectric ultrasonic motor (PUM) driven stage consists of two PUMs, shown in Fig. 1. The PUM moving along the Y-axis is orthogonally mounted on the PUM moving along the X-axis, *i.e.*, the stator (base) of Y-axis PUM is connected to the mover of X-axis PUM via threaded fasteners. Due to the series connection between the two PUMs, there is no motion along Y-axis when only the X-axis PUM is driven, while there is motion along X-axis because of interacting friction force when only the Y-axis PUM is driven. The coupling effect exists in this X–Y stage.

For each PUM, the piezoelectric component induced in the stator is used both to impart motion and to modulate the frictional forces present at the interface, and the output platform is bonded on the mover moving along the linear guide. The ultrasonic vibration of the piezoelectric component can power the motion of the moving end. During the motion, the friction at the interface between the moving end and the corresponding unmoving base arises and results the system affected by nonlinearity.

2.1.1. Y-axis

The Y-axis PUM acts as a single-axis PUM. In [35], the hysteresis, creep, cross-coupling, and external disturbance are consolidated into an output disturbance. Similar to the modeling approach in [35], the unmodeled uncertainty and disturbance are treated as a total disturbance. The following dynamic model is used to describe it [23]:

$$\ddot{y}(t) + \mathrm{a}_{y1}\dot{y}(t) + \mathrm{a}_{y0}y(t) = \mathrm{b}_{y0}u_y(t) + f_y(t) + d_y(t), \tag{1}$$

where u_y and y are the control input and position output, respectively. a_{y1}, a_{y0}, and b_{y0} are the model coefficients. f_y is the nonlinear term and d_y is disturbance.

The nonlinear term is resulted from the characteristics of the piezoelectric component and the drive mechanism, including hysteresis and friction. Frictional force at the interface is the major nonlinear component of this PUM. In this paper, the nonlinear term is described by a Coulomb friction model f_{yc} added to an uncertain nonlinear component Δf_y.

$$f_y(t) = f_{yc}(t) + \Delta f_y(t). \tag{2}$$

It is found from the open loop test that, the friction is asymmetric in forward and backward motions [23]. Thus the model of the nonlinear term can be modeled by Coulomb friction plus a constant,

$$f_{yc}(t) = \mathrm{f}_{y1}\,\mathrm{sign}(\dot{y}) + \mathrm{f}_{y2}, \tag{3}$$

where 'sign' is the signum function, and $\mathrm{f}_{y1}, \mathrm{f}_{y2}$ are unknown model coefficients.

In practical situation, the bounded model uncertainty and disturbance are combined into $p_y(t)$,

$$p_y(t) = \Delta f_y(t) + d_y(t). \tag{4}$$

2.1.2. X-axis

Due to the physical configuration of the stage, the dynamics of the X-axis PUM is affected by the coupling with Y-axis motion. Considering the motion principle of PUM, the friction force drives the moving end, X-axis motion is also partly affected by the friction force of Y-axis when the two axes are non-orthogonal and interact with each other. The dynamics model of the X-axis PUM can be expressed as:

$$\ddot{x}(t) + \mathrm{a}_{x1}\dot{x}(t) + \mathrm{a}_{x0}x(t) = \mathrm{b}_{x0}u_x(t) + f_x(t) + f_{yx}(t) + d_x(t), \tag{5}$$

where f_{yx} is the coupling from Y-axis motion to X-axis, x is the output displacement, and other corresponding parameters have the same definitions like those for Y-axis.

$$f_x(t) = f_{xc}(t) + \Delta f_x(t), \tag{6}$$

$$f_{xc}(t) = \mathrm{f}_{x1}\mathrm{sign}(\dot{x}) + \mathrm{f}_{x2}, \tag{7}$$

$$f_{yx}(t) = \mathrm{c}_1\mathrm{sign}(\dot{y}) + \mathrm{c}_2, \tag{8}$$

where $\mathrm{f}_{x1}, \mathrm{f}_{x2}, \mathrm{c}_1, \mathrm{c}_2$ are unknown model coefficients.

The bounded model uncertainty and disturbance are combined into a single variable $p_x(t)$,

$$p_x(t) = \Delta f_x(t) + d_x(t). \tag{9}$$

2.2. Control problem statement

The dynamic models (1) of Y-axis and (5) X-axis are rewritten as

$$\ddot{y}(t) + \mathrm{a}_{y1}\dot{y}(t) + \mathrm{a}_{y0}y(t) = \mathrm{b}_{y0}u_y(t) + f_{yc}(t) + p_y(t), \tag{10}$$

$$\ddot{x}(t) + \mathrm{a}_{x1}\dot{x}(t) + \mathrm{a}_{x0}x(t) = \mathrm{b}_{x0}u_x(t) + f_{xc}(t) + f_{yx}(t) + p_x(t). \tag{11}$$

The system model can be expressed in a matrix form,

$$\ddot{\boldsymbol{q}} + \mathbf{B}\dot{\boldsymbol{q}} + \mathbf{K}\mathbf{q} = \mathbf{T}\boldsymbol{u} + \mathbf{F}\mathbf{S}(\dot{\boldsymbol{q}}) + \mathbf{d}_n + \boldsymbol{d}, \tag{12}$$

for conciseness, where $\boldsymbol{q} = [y(t),\ x(t)]^T$, $\dot{\boldsymbol{q}} = [\dot{y}(t),\ \dot{x}(t)]^T$, and $\ddot{\boldsymbol{q}} = [\ddot{y}(t),\ \ddot{x}(t)]^T$ are the vectors of the axis position, velocity and acceleration, respectively. $\boldsymbol{u} = [u_y(t),\ u_x(t)]^T$ is the control input, $\mathbf{S}(\dot{\boldsymbol{q}}) = [\mathrm{sign}(\dot{y}),\ \mathrm{sign}(\dot{x})]^T$ is a sign function of the velocity, $\mathbf{d}_n = [\mathrm{f}_{y2},\ \mathrm{f}_{x2}{+}\mathrm{c}_2]^T$ is the nominal value of the unknown nonlinearity, and $\boldsymbol{d} = [p_y(t),\ p_x(t)]^T$ is the residual disturbance. The disturbance $\boldsymbol{d}$ is assumed to be bounded $|\boldsymbol{d}| \le \mathbf{d}_M$. $\mathbf{B} = \mathrm{diag}[\mathrm{a}_{y1},\ \mathrm{a}_{x1}]$, $\mathbf{K} = \mathrm{diag}[\mathrm{a}_{y0},\ \mathrm{a}_{x0}]$, $\mathbf{T} = \mathrm{diag}[\mathrm{b}_{y0},\ \mathrm{b}_{x0}]$, and $\mathbf{F} = [\mathrm{f}_{y1},\ 0;\ \mathrm{c}_1,\ \mathrm{f}_{x1}]$ are matrices of model coefficients, where $\mathrm{diag}(\bullet)$ is a function that convert a vector $\bullet$ to a diagonal matrix.

The control objectives are: (1) to achieve precise tracking of reference trajectory $y_d(t)$ for Y-axis by handling the adverse effects nonlinear frictional force $f_{yc}(t)$ and disturbance $p_y(t)$; (2) to achieve a precise tracking of $x_d(t)$ for X-axis in the presence of nonlinear friction $f_{xc}(t)$, unilateral coupling $f_{yx}(t)$ and disturbance $p_x(t)$. Design of an ASMC control scheme based on PID-type sliding mode to achieve these control objectives is presented in the next section.

3. Controller design

To overcome these control issues, an adaptive robust controller is designed. Let us define the position error,

$$\boldsymbol{e}(t) = \boldsymbol{q}(t) - \boldsymbol{q}_d(t), \tag{13}$$

where $\boldsymbol{q}_d(t) = [y_d(t),\ x_d(t)]^T$ is the desired position trajectories.

A PID type of sliding mode function based on the error (13) can be designed as:

$$\boldsymbol{\sigma}(t) = [\sigma_y,\ \sigma_x]^T = \dot{\boldsymbol{e}}(t) + \mathbf{k}_1\boldsymbol{e}(t) + \mathbf{k}_2\int_0^t \boldsymbol{e}(\tau)d\tau, \tag{14}$$

where $\mathbf{k}_1 = \mathrm{diag}[\mathrm{k}_{y1},\ \mathrm{k}_{x1}]$ and $\mathbf{k}_2 = \mathrm{diag}[\mathrm{k}_{y2},\ \mathrm{k}_{x2}]$ are control gain matrices. It is easy to tune the control gains according to the rule that the characteristic polynomial $s^2 + \mathrm{k}_{y1}s + \mathrm{k}_{y2} = 0$ and $s^2 + \mathrm{k}_{x1}s + \mathrm{k}_{x2} = 0$ need to be strictly Hurwitz, where s is the Laplace operator, *i.e.*, the roots of the polynomials are with negative real parts. The gains are selected as positive values in the subsequent experiments.

Theorem 1. *For the system synthesized by (12), if the controller (15) is adopted, the system can maintain robustness and enable the position tracking error converging to zero asymptotically.*

$$\begin{aligned}\boldsymbol{u} &= \mathbf{T}^{-1}[\ddot{\boldsymbol{q}}_d + \hat{\mathbf{B}}\dot{\boldsymbol{q}} + \hat{\mathbf{K}}\boldsymbol{q} - \hat{\mathbf{F}}\mathbf{S}(\dot{\boldsymbol{q}}) - \hat{\mathbf{d}}_n \\ &\quad - \mathbf{k}_1\dot{\boldsymbol{e}} - \mathbf{k}_2\boldsymbol{e} - \mathbf{k}_s\boldsymbol{\sigma} - \boldsymbol{\beta}\mathrm{sign}(\boldsymbol{\sigma})] \\ &= \mathbf{T}^{-1}[\boldsymbol{u}_a - \mathbf{k}_1\dot{\boldsymbol{e}} - \mathbf{k}_2\boldsymbol{e} - \mathbf{k}_s\boldsymbol{\sigma} - \boldsymbol{\beta}\mathrm{sign}(\boldsymbol{\sigma})],\end{aligned} \tag{15}$$

where $\hat{\bullet}$ is the estimated value of $\bullet$, and $\mathbf{k}_s = \mathrm{diag}[\mathrm{k}_{ys}\ ,\mathrm{k}_{xs}]$ and $\boldsymbol{\beta} = \mathrm{diag}(\mathcal{B})$ with $\mathcal{B} = [\beta_y,\ \beta_x]^T$ are positive control parameters that are designed to be $\mathcal{B} \ge \mathbf{d}_M + \mathcal{H}$, and $\mathcal{H} = [\eta_y,\ \eta_x]^T$ is a vector contains the diagonal elements of a designed positive diagonal matrix $\boldsymbol{\eta}$ that can be arbitrarily small, i.e., $\boldsymbol{\eta} = \mathrm{diag}(\mathcal{H})$. $\boldsymbol{u}_a$ consists of the desired trajectory and the model-based adaptive compensation, where the desired trajectory is usually known in advance.

Proof of Theorem 1. The model based adaptive control term is presented in detail,

$$\boldsymbol{u}_a = \ddot{\boldsymbol{q}}_d + \hat{\mathbf{B}}\dot{\boldsymbol{q}} + \hat{\mathbf{K}}\boldsymbol{q} - \hat{\mathbf{F}}\mathbf{S}(\dot{\boldsymbol{q}}) - \hat{\boldsymbol{d}}_n = [u_{ya}\ u_{xa}]^T. \tag{16}$$

For clearer presentation, the corresponding control laws u_{ya} for Y-axis and u_{xa} for X-axis are expanded as follows.

$$\begin{aligned}u_{ya} &= \ddot{y}_d + \hat{\mathrm{a}}_{y1}\dot{y} + \hat{\mathrm{a}}_{y0}y - \hat{f}_{yc} \\ &= \ddot{y}_d + \hat{\mathrm{a}}_{y1}\dot{y} + \hat{\mathrm{a}}_{y0}y - \hat{\mathrm{f}}_{y1}\mathrm{sign}(\dot{y}) - \hat{\mathrm{f}}_{y2} \\ &= \ddot{y}_d + \boldsymbol{\phi}_y\hat{\boldsymbol{\theta}}_y,\end{aligned} \tag{17}$$

$$\dot{\hat{\boldsymbol{\theta}}}_y = -\boldsymbol{\Gamma}_y\boldsymbol{\phi}_y^T\sigma_y, \tag{18}$$

where $\boldsymbol{\phi}_y = [\dot{y}\ y\ \ -\mathrm{sign}(\dot{y})\ \ -1]$ and $\boldsymbol{\theta}_y = [\mathrm{a}_{y1}\ \mathrm{a}_{y0}\ \mathrm{f}_{y1}\ \mathrm{f}_{y2}]^T$. $\hat{\boldsymbol{\theta}}_y$ denotes the estimated value of $\boldsymbol{\theta}_y$ and $\tilde{\boldsymbol{\theta}}_y$ is the estimation error ($\tilde{\boldsymbol{\theta}}_y = \hat{\boldsymbol{\theta}}_y - \boldsymbol{\theta}_y$) and $\boldsymbol{\Gamma}_y$ is the diagonal adaptation rate matrix.

Similar control design process is used for the X-axis, in which the coupling is taken into account.

$$\begin{aligned}u_{xa} &= \ddot{x}_d + \hat{\mathrm{a}}_{x1}\dot{x} + \hat{\mathrm{a}}_{x0}x - \hat{f}_{xc} - \hat{f}_{yx} \\ &= \ddot{x}_d + \hat{\mathrm{a}}_{x1}\dot{x} + \hat{\mathrm{a}}_{x0}x - \hat{\mathrm{f}}_{x1}\mathrm{sign}(\dot{x}) - \hat{\mathrm{f}}_{x2} \\ &\quad - \hat{\mathrm{c}}_1\mathrm{sign}(\dot{y}) - \hat{\mathrm{c}}_2 \\ &= \ddot{x}_d + \boldsymbol{\phi}_x\hat{\boldsymbol{\theta}}_x,\end{aligned} \tag{19}$$

$$\dot{\hat{\boldsymbol{\theta}}}_x = -\boldsymbol{\Gamma}_x\boldsymbol{\phi}_x^T\sigma_x, \tag{20}$$

where $\boldsymbol{\phi}_x = [\dot{x}\ x\ -\mathrm{sign}(\dot{x})\ -\mathrm{sign}(\dot{y})\ -1]$ and $\boldsymbol{\theta}_x = [\mathrm{a}_{x1}\ \mathrm{a}_{x0}\ \mathrm{f}_{x1}\ c_1\ \mathrm{f}_{x2}{+}\mathrm{c}_2]^T$. $\hat{\boldsymbol{\theta}}_x$ denotes the estimate of $\boldsymbol{\theta}_x$, and $\boldsymbol{\Gamma}_x$ is the diagonal adaptation rate matrix.

To facilitate the subsequent stability analysis of the system with the control, a Lyapunov function V is chosen as

$$V(t) = \frac{1}{2}\boldsymbol{\sigma}^T\boldsymbol{\sigma} + \frac{1}{2}\tilde{\boldsymbol{\theta}}_y^T\boldsymbol{\Gamma}_y^{-1}\tilde{\boldsymbol{\theta}}_y + \frac{1}{2}\tilde{\boldsymbol{\theta}}_x^T\boldsymbol{\Gamma}_x^{-1}\tilde{\boldsymbol{\theta}}_x. \tag{21}$$

With the system model (12) and the control law (15), it can be obtained,

$$\begin{aligned}\dot{\boldsymbol{\sigma}} &= \ddot{\boldsymbol{e}} + \mathbf{k}_1\dot{\boldsymbol{e}} + \mathbf{k}_2\boldsymbol{e} \\ &= (\hat{\mathbf{B}} - \mathbf{B})\dot{\boldsymbol{q}} + (\hat{\mathbf{K}} - \mathbf{K})\boldsymbol{q} - (\hat{\mathbf{F}} - \mathbf{F})\mathbf{S}(\dot{\boldsymbol{q}}) - (\hat{\boldsymbol{d}}_n - \boldsymbol{d}_n) + \boldsymbol{d} - \mathbf{k}_s\boldsymbol{\sigma} - \boldsymbol{\beta}\mathrm{sign}(\boldsymbol{\sigma}) \\ &= \tilde{\mathbf{B}}\dot{\boldsymbol{q}} + \tilde{\mathbf{K}}\boldsymbol{q} - \tilde{\mathbf{F}}\mathbf{S}(\dot{\boldsymbol{q}}) - \tilde{\boldsymbol{d}}_n + \boldsymbol{d} - \mathbf{k}_s\boldsymbol{\sigma} - \boldsymbol{\beta}\mathrm{sign}(\boldsymbol{\sigma})\end{aligned} \tag{22}$$

where, $\tilde{\bullet} = \hat{\bullet} - \bullet$.

Taking the derivative of (21), and taking into account (22), the adaptive rules (18) and (20), the resulting expression can be simplified to

$$\begin{aligned}\dot{V} &= \boldsymbol{\sigma}^T\dot{\boldsymbol{\sigma}} + \tilde{\theta}_y^T\Gamma_y^{-1}\dot{\hat{\theta}}_y + \tilde{\theta}_x^T\Gamma_x^{-1}\dot{\hat{\theta}}_x \\ &= \boldsymbol{\sigma}^T[\tilde{\mathbf{B}}\dot{q} + \tilde{\mathbf{K}}q - \tilde{\mathbf{F}}\mathrm{S}(\dot{q}) - \tilde{d}_n + d - \mathbf{k}_s\boldsymbol{\sigma} - \beta\mathrm{sign}(\boldsymbol{\sigma})] \\ &\quad - \tilde{\theta}_y^T\phi_y^T\sigma_y - \tilde{\theta}_x^T\phi_x^T\sigma_x \\ &= \boldsymbol{\sigma}^T[\tilde{\mathbf{B}}\dot{q} + \tilde{\mathbf{K}}q - \tilde{\mathbf{F}}\mathrm{S}(\dot{q}) - \tilde{d}_n + d - \mathbf{k}_s\boldsymbol{\sigma} - \beta\mathrm{sign}(\boldsymbol{\sigma})] \\ &\quad - \boldsymbol{\sigma}^T[\tilde{\theta}_y^T\phi_y^T, \tilde{\theta}_x^T\phi_x^T]^T \\ &= \boldsymbol{\sigma}^T(d - \mathbf{k}_s\boldsymbol{\sigma} - \beta\mathrm{sign}(\boldsymbol{\sigma})).\end{aligned} \tag{23}$$

If β is chosen to hold the inequality $\mathcal{B} \geq \mathbf{d}_M + \mathcal{H}$, then,

$$\begin{aligned}\dot{V} &= \boldsymbol{\sigma}^T(d - \mathbf{k}_s\boldsymbol{\sigma} - \beta\mathrm{sign}(\boldsymbol{\sigma})) \\ &\leq |\boldsymbol{\sigma}^T|(\mathbf{d}_M - \mathbf{k}_s|\boldsymbol{\sigma}| - \mathcal{B}) \\ &\leq -\mathbf{k}_s\|\boldsymbol{\sigma}\|^2 + |\boldsymbol{\sigma}^T|(\mathbf{d}_M - \mathcal{B}) \\ &\leq -\mathbf{k}_s\|\boldsymbol{\sigma}\|^2 - |\boldsymbol{\sigma}^T|\mathcal{H} \\ &\leq -\mathbf{k}_s\|\boldsymbol{\sigma}\|^2 \leq 0.\end{aligned} \tag{24}$$

When the parameters are chosen to satisfy the inequality mentioned previously, it can be obtained that the time derivative of the Lyapunov function has been proved to be semi-negative definite, which implies that $\boldsymbol{\sigma}$, $\tilde{\theta}_y$ and $\tilde{\theta}_x$ are bounded with respect to time.

It can be also observed that $\dot{\boldsymbol{\sigma}}$ is bounded because $\boldsymbol{\sigma}$, $\hat{\theta}_y$ and $\hat{\theta}_x$ are bounded. Then, from (24), we have

$$\lim_{t\to\infty}\int_0^t \mathbf{k}_s\|\boldsymbol{\sigma}\|^2\tau \leq -V(\infty) + V(0) \leq V(0), \tag{25}$$

where the positive definiteness of V has been used. By virtue of Barbalat's lemma, we can conclude that

$$\lim_{t\to\infty}\|\boldsymbol{\sigma}(t)\| = 0. \tag{26}$$

Therefore, it can be concluded that the stability and the convergence of tracking error will be guaranteed through employing the proposed controller.

Remark 1. In the control law, $\boldsymbol{u}_a$ is obtained using the dynamic model and functions as the adjustable model compensation to handle the nonlinear friction force for an improved tracking accuracy. The robust control part of the control law in equation (15) is composed of a linear feedback term $-\mathbf{k}_1\dot{e} - \mathbf{k}_2 e - \mathbf{k}_s\boldsymbol{\sigma}$ with $\mathbf{k}_s > 0$ to stabilize the nominal system, and the variable structure sliding mode control law $\beta\mathrm{sign}(\boldsymbol{\sigma})$ to attenuate the effect of estimation error.

Remark 2. When the parameter matrix $\mathbf{k}_s$ is set large to satisfy $|d| - \mathbf{k}_s|\sigma| \leq 0$, the control law can guarantee stability of the system without the term $\beta\mathrm{sign}(\boldsymbol{\sigma})$. This means that β can be chosen as a small value to avoid the chattering problem of traditional SMC when $\mathbf{k}_s$ is set to a larger value within the suitable range.

The proposed adaptive robust control scheme is illustrated by the block diagram shown in Fig. 2.

To apply the controller in practice, the tuning parameters are gains $\mathbf{k_1}, \mathbf{k_2}, \mathbf{k_s}, \beta$ and adaptation rates Γ_x, Γ_y, whose settings are shown as follows.

The reaching law can be derived from the control law (15) as,

$$\dot{\boldsymbol{\sigma}} = -\mathbf{k}_s\boldsymbol{\sigma} - \beta\mathrm{sign}(\boldsymbol{\sigma}), \tag{27}$$

where $\mathbf{k_s}$ and β in (27) are associated with the control stability and the rate of reaching the sliding mode surface. They are both diagonal matrices with positive constants.

Remark 3. If $\mathcal{B} \geq |d|$, it can be seen that the system is stable as long as $\mathbf{k}_s \geq 0$. $\mathbf{k}_s$ is the key to affect the rate of reaching the sliding mode surface. However, $\beta\mathrm{sign}(\boldsymbol{\sigma})$ is a discontinuous term, large value of β may cause chattering problem. To avoid this issue, β needs to be set as small as possible. Taking into account the stability and rapidity of convergence, β takes a smaller value and $\mathbf{k}_s$ takes a larger value so that the controller can achieve high tracking performance.

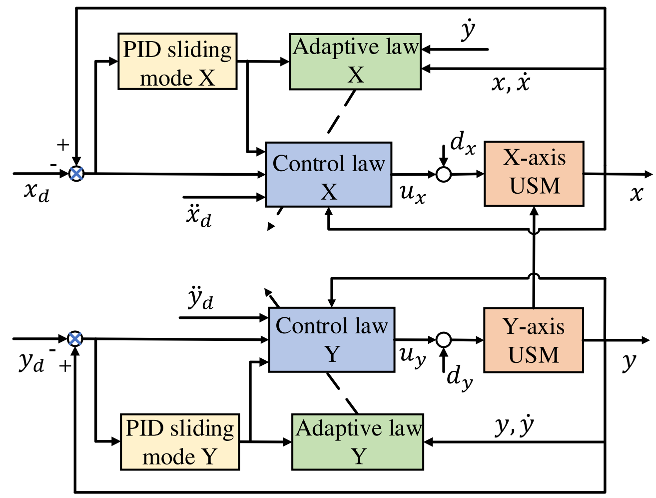

Fig. 2. Block diagram of the proposed control scheme.

Remark 4. $\mathbf{k}_1$ and $\mathbf{k}_2$ in (14) are related to the dynamic convergence characteristics of the output displacement tracking performance, which should be chosen as positive diagonal matrices to meet Hurwitz stability criterion.

Remark 5. The adaptation rates Γ_x, Γ_y have influences on the estimation speed of the unknown model coefficients $\mathbf{B}, \mathbf{K}, \mathbf{F}, \boldsymbol{d_n}$. If they are small, the estimation error will converge slowly. On the contrary, too large value results in the estimation value vibrating sharply. These parameters can be chosen empirically and adjusted in experiments for better performance.

4. Experimental setup

4.1. Experimental system

Fig. 3 show the experimental setup. The system consists of two PUMs (model: C-185, from Physik Instrumente Co., Ltd.) to realize X and Y direction motion. Each PUM has a stroke limit of ±10 mm, and the integrated linear encoder used for output displacement measurement has a resolution of 0.1 μm. A dSPACE DS1104 embedded rapid prototyping system is employed to implement the controller with a sampling frequency of 1 kHz. A control PC is used to realize real-time interface and control.

4.2. System identification

In order to identify the nominal model of the stage, an input signal containing multiple frequency components is applied. The input–output data is collected and imported to MATLAB for identification. Interested readers may refer to an earlier publication [8] for details. Identified transfer functions are:

$$G_y = \frac{2299}{s^2 + 182.7s + 460.8} \tag{28}$$

and

$$G_x = \frac{4940}{s^2 + 202s + 248.4}. \tag{29}$$

The corresponding coefficients $b_{y0} = 2299,\ a_{y1} = 182.7,\ a_{y0} = 460.8$ and $b_{x0} = 4940,\ a_{x1} = 202,\ a_{x0} = 248.4$ will be used in the controllers.

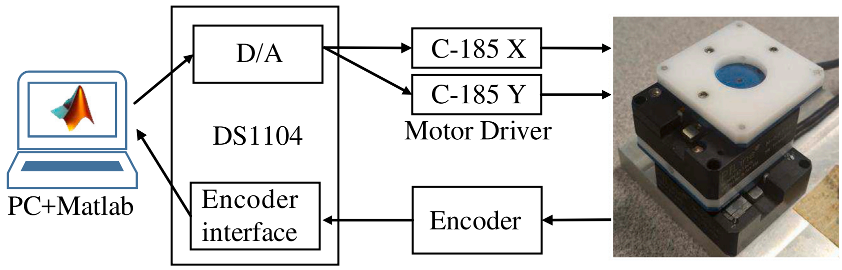

Fig. 3. Experimental setup.

4.3. Controller implementation

To conduct a comparison, three different controllers are designed and implemented: (1) proposed ASMC, (2) conventional PID control, and (3) SMC based on PID-sliding mode assisted by ESO.

ASMC: This is the adaptive SMC proposed in this paper. The controller parameters are $\mathbf{k}_1 = \mathbf{k}_2 = \mathbf{k}_s = \text{diag}[w_{cy}\ w_{cx}]$ with $w_{cy} = 2\pi \times 80, w_{cx} = 2\pi \times 100$ and $\boldsymbol{\beta} = \text{diag}[0.001\ 0.001]$ and the adaptive rates are $\boldsymbol{\Gamma}_y$= diag[10 10 1000 10], and $\boldsymbol{\Gamma}_x$ = diag[10 10 1000 10 1]. The initial values of the adaptive dynamic model parameters are set as the identified values. The initial values of the nonlinear term coefficients and disturbances are set to zero.

It should be noted that the coupling effect in the 2-DOF stage is unilateral coupling, not cross coupling. The designed control is not cross-coupled control, so there is no control allocation problem in the experiments.

PID: Proportional–Integral–Derivative controller is widely used in the industry. To ensure that the feedback gains are identical with the proposed controller, the PID parameters are set as $\mathbf{k}_p = \text{diag}[w_{cy}^2\ w_{cx}^2]$, $\mathbf{k}_i = \text{diag}[w_{cy}^2 + w_{cy}\ w_{cx}^2 + w_{cx}]$, and $\mathbf{k}_d = \text{diag}[2w_{cy}\ 2w_{cx}]$.

$$\boldsymbol{u}_{PID} = -\mathbf{T}^{-1}(\mathbf{k}_p\mathbf{e} + \mathbf{k}_i \int \mathbf{e} + \mathbf{k}_d\dot{\mathbf{e}}). \tag{30}$$

where $\mathbf{T} = \text{diag}[b_{y0},\ b_{x0}]$.

SMC-ESO: The sliding mode control (SMC) with extended state observer (ESO) is selected as an advanced comparative controller. It has been successfully used in many applications as previously mentioned [11,12,21]. This controller also has advantage in dealing with model uncertainties and disturbances. The controller is redesigned in this paper, based on the same PID-type sliding mode. The unmodeled nonlinear term and disturbance is treated as an extra state of the system, and ESO is used to estimate and compensate it.

For simplicity, the system model for X and Y axes can be unified as

$$\ddot{x}(t) + \mathrm{a}_1\dot{x}(t) + \mathrm{a}_0 x(t) = \mathrm{b}_0 u(t) + a(t), \tag{31}$$

where $a(t)$ includes all the model uncertainties and disturbance. $\hat{a}(t)$ is estimated by the ESO.

Then the estimated $\hat{a}(t)$ is used as an ESO control law, and the SMC is implemented same as the proposed controller but without parameters adaptation. The resulting SMC-ESO controller is determined by

$$\begin{aligned} u &= u_1 + u_a + u_s, \\ u_1 &= -\frac{1}{\mathrm{b}_0}\hat{\mathrm{a}}(t), \\ u_a &= \frac{1}{\mathrm{b}_0}[\ddot{x}_d + \mathrm{a}_1\dot{x} + \mathrm{a}_0 x], \\ u_s &= -\mathrm{k}_s\sigma_x - \mathrm{k}_1\dot{e} - \mathrm{k}_2 e - \beta\text{sign}(\sigma), \end{aligned} \tag{32}$$

where $e = x - x_d, \sigma = \dot{e} + \mathrm{k}_1 e + \mathrm{k}_2 \int e$. For fair comparison, all gains of the feedback control term are chosen the same as those of PID and ASMC. The controller parameters are $\mathrm{k}_1 = w_c, \mathrm{k}_2 = w_c, \mathrm{k}_s = w_c$, and $\beta = 0.001$. The observer bandwidth w_0 is the only parameter for the ESO and the value can be larger to estimate the disturbance more accurately. But the estimation accuracy is influenced by the noise. It is set as $w_0 = 2 * \pi * 150$ in experiments by trial and error.

5. Experimental results

Comparison of performances of three different controllers are carried out through several experiments. For comparison, we consider the root-mean-square (RMS) error μ_e, the maximum tracking error M_e, and the average composition error A_e, which are defined as,

$$\begin{aligned} \mu_e &= \sqrt{\frac{1}{\mathrm{N}}\sum_{i=1}^{\mathrm{N}} e_i^2}, \\ M_e &= \max(|e|), \\ A_e &= \frac{1}{\mathrm{N}}\sum_{i=1}^{\mathrm{N}} \sqrt{e_x^2 + e_y^2}. \end{aligned} \tag{33}$$

where N is the number of data samples used.

5.1. Coupling compensation

To verify the coupling compensation effect of the proposed controller, a sine wave $y_d = \sin(2\pi * 10t)$ is used for the motion along the Y-axis while keeping the X-axis with zero input. The X-axis position outputs in open-loop and closed-loop are shown in Figs. 4(b) and 4(c) respectively. It can be seen that in closed-loop the X-axis with the proposed controller can effectively suppress the coupling error from Y-axis to X-axis. Then a circular motion is conducted, the reference trajectories are $y_d = \sin(2\pi * 10t)$ and $x_d = 1 - \cos(2\pi * 10t)$. In case 1, the controller for X-axis is implemented without coupling adaption (i.e., $f_{yx} = 0$), while in case 2 it is implemented with coupling adaption. The tracking errors in the two cases are shown in Fig. 5. The RMS errors of X-axis are 0.0074 mm in case 1 and 0.0068 mm in case 2. It can be seen that considering coupling effect during design helps to improve the tracking accuracy of X-axis by 8.1%. The improvement is not obvious, which can be explained in two aspects: (a) the coupling effect is small compared with the control input; (b) the controller designed with high gain feedback control term can address such coupling as disturbance effectively.

5.2. Sine wave trajectory (circular motion)

In this experiment, the 2-DOF stage is controlled to track several circular motions. The performance indexes are collected in Table 1. It is easily observed, by comparing the results of PID and SMC-ESO, that ESO gives significant improvement in tracking accuracy by compensating the disturbance using the additional estimated state. However, with increasing frequency of circular motion, the tracking performance with SMC-ESO becomes worse because of the bandwidth limitation. When the reference changes fast, the ESO cannot estimate the lump disturbance accurately enough. On the contrary, the ASMC can hold high accuracy in fast changing reference tracking. Among the three controllers, ASMC has the best performance, the RMS errors of the 1–10 Hz reference signals are within 10 μm. In ASMC, the PID-type sliding mode provides a robust feedback control. On the basis of this, adaptive control is combined to improve the accuracy by using adaptation of the unknown model parameters to compensate nonlinearities and

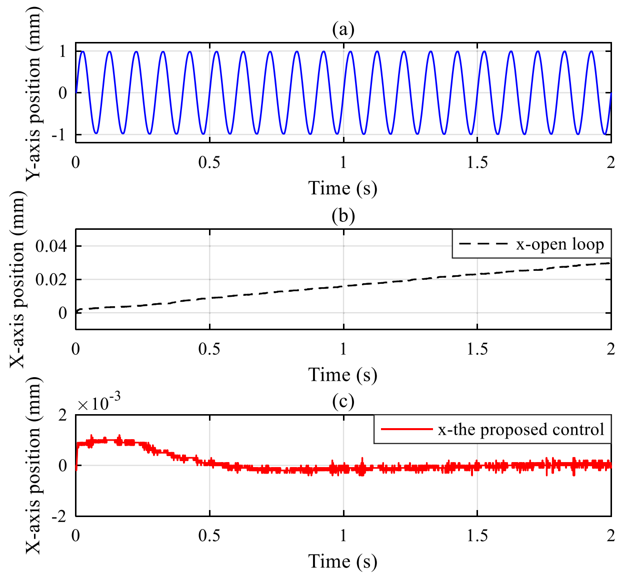

Fig. 4. Position outputs comparison of open-loop and closed-loop.

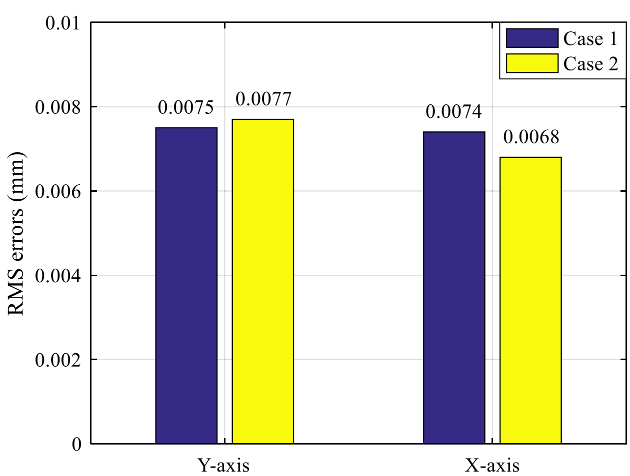

Fig. 5. Tracking errors comparison of with and without consideration of coupling.

uncertainties. The experimental results show that adaptive control is suitable for a class of systems with known structure but uncertain model parameters.

The experimental results of the circular trajectory (1 mm and 10 Hz) are shown in Figs. 6 and 7 for clear comparison. The proposed controller achieves better performance than the other two controllers in terms of transient and tracking accuracy. It is observed that the adaptive control can compensate nonlinear friction and model uncertainties effectively to achieve the best tracking performance with the same high gain feedback control. The circular motion is shown in Fig. 8.

5.3. Triangular wave trajectory

Besides, the experiment results of triangle waves have been conducted. Due to triangular waves containing high frequency harmonics, the reference with the frequency of 1 Hz and 2 Hz has been used in the experiments. The value of RMSE and MAXE tracking errors are listed in Table 2. The compared tracking results of triangle wave (2 Hz, 2 mm) are shown the Fig. 9.

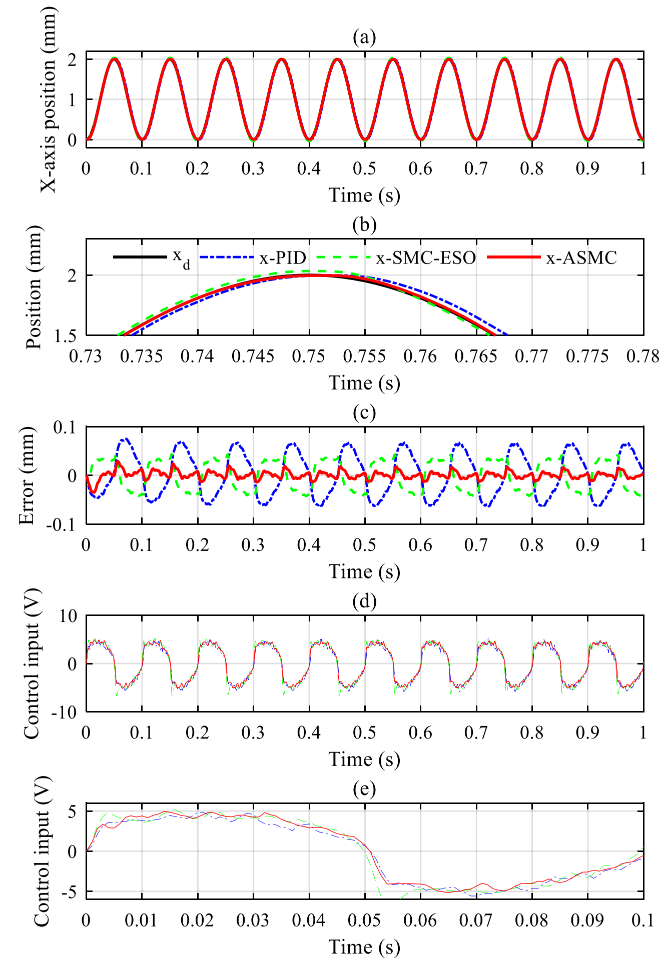

Fig. 6. Tracking results comparison of X-axis on circular trajectory (1 mm, 10 Hz).

Table 1
Circular motion tracking errors.

Freq (Hz)	Errors (μm)	PID		SMC-ESO		ASMC	
		X	Y	X	Y	X	Y
1	μ_e	10.85	10.37	6.86	6.89	2.59	2.84
	M_e	27.70	28.67	11.00	11.85	6.20	7.99
	A_e	13.69		9.68		3.64	
5	μ_e	31.52	30.99	20.17	23.27	5.51	5.69
	M_e	47.83	48.58	30.65	30.45	15.22	13.19
	A_e	43.78		30.16		7.26	
10	μ_e	45.96	46.50	31.53	33.49	6.76	7.68
	M_e	67.21	70.57	42.72	45.01	17.42	18.32
	A_e	65.12		45.57		9.23	

Table 2
Indexes of triangular wave tracking.

Freq (Hz)	1		2	
Errors (μm)	μ_e	M_e	μ_e	M_e
PID	12.07	36.82	21.85	50.83
SMC-ESO	7.73	30.87	19.01	42.89
ASMC	3.74	18.12	4.19	31.92

5.4. Robustness test

To verify the proposed controller can deal with disturbance robustly, the extreme disturbance $dis = 0.1 + 0.01\sin(2\pi t - \pi/6) + 0.01\sin(10\pi t)$ is randomly selected and applied to X-axis in the experiments. Fig. 10 shows the compared tracking results for 10 Hz sine wave

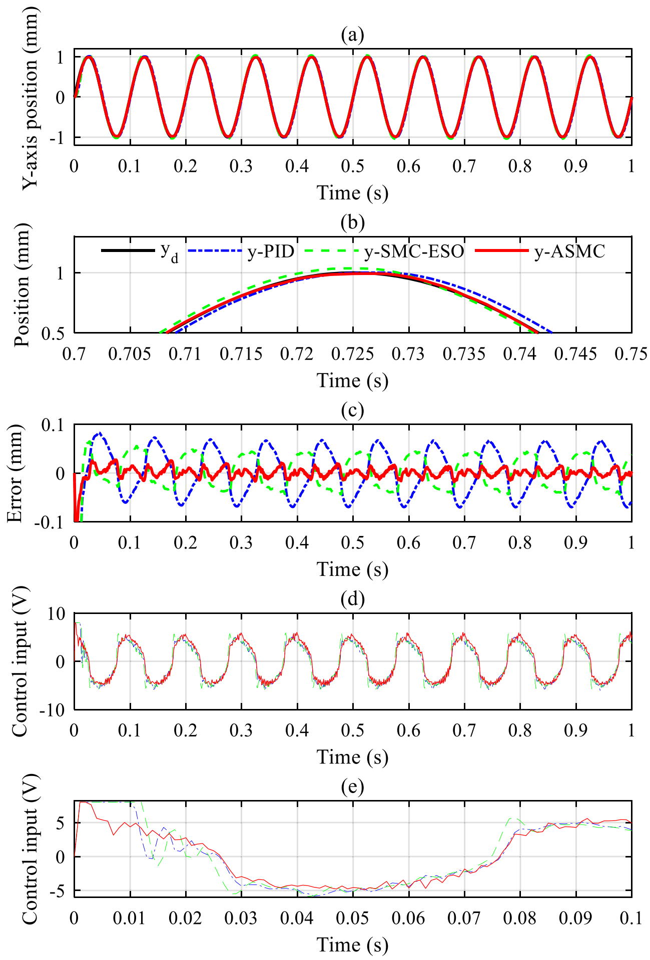

Fig. 7. Tracking results comparison of Y-axis on circular trajectory (1 mm, 10 Hz).

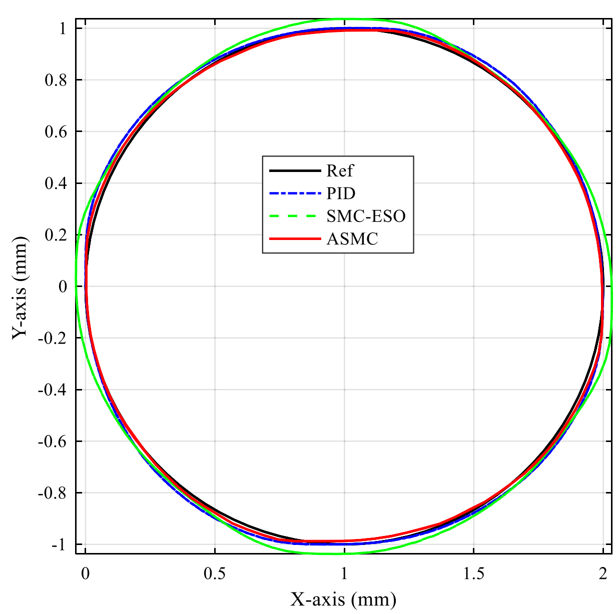

Fig. 8. Circular motion (1 mm, 10 Hz).

reference trajectory, and the error bars shown in Fig. 11 compares the tracking performance of the controller with and without the extreme disturbance. It can be noted that the proposed method can reduce the

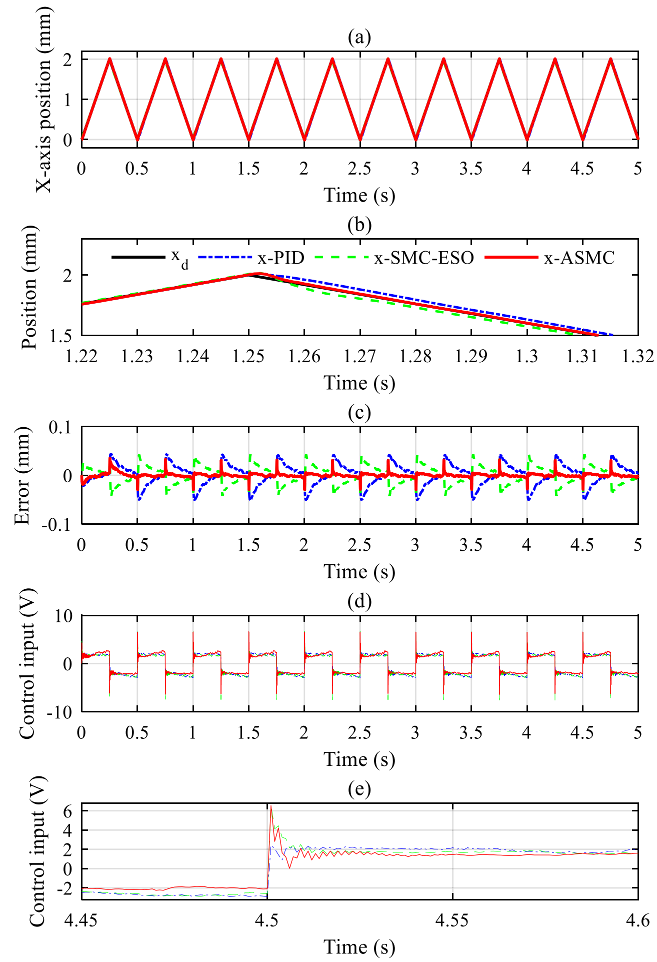

Fig. 9. Tracking results comparison of X-axis with of triangular wave (2 Hz, 2 mm).

Table 3
Indexes of robustness test against the extreme disturbance.

Freq (Hz)	1		5		10	
Errors (μm)	μ_e	M_e	μ_e	M_e	μ_e	M_e
PID	11.65	28.83	33.51	50.82	49.51	72.23
SMC-ESO	6.92	13.24	29.97	42.75	32.23	43.41
ASMC	2.54	7.68	4.59	14.42	7.32	16.74

impact of interference and achieve satisfied tracking accuracy. Table 3 gives the values of performance indexes.

5.5. Specified motion

Furthermore, to investigate the performance of the proposed controller in practical application, a specified motion trajectory (for an ear surgical operation) is chosen as an example, like that in [8]. Figs. 12 and 13 show the tracking results of the three comparative controllers. The performance indexes are collected in Table 4. For the tracking performance of ASMC, μ_e for X-axis and Y-axis are 3.41 μm and 3.68 μm, respectively. As seen in these data and figures, the proposed ASMC is valid for practical application and performs the best among the three controllers for the specified motion. (See Fig. 14.)

6. Conclusion

In this paper, a nonlinear adaptive robust controller with PID-type sliding mode is developed to deal with nonlinear friction and parametric uncertainties and coupling effects for a 2-DOF stage driven

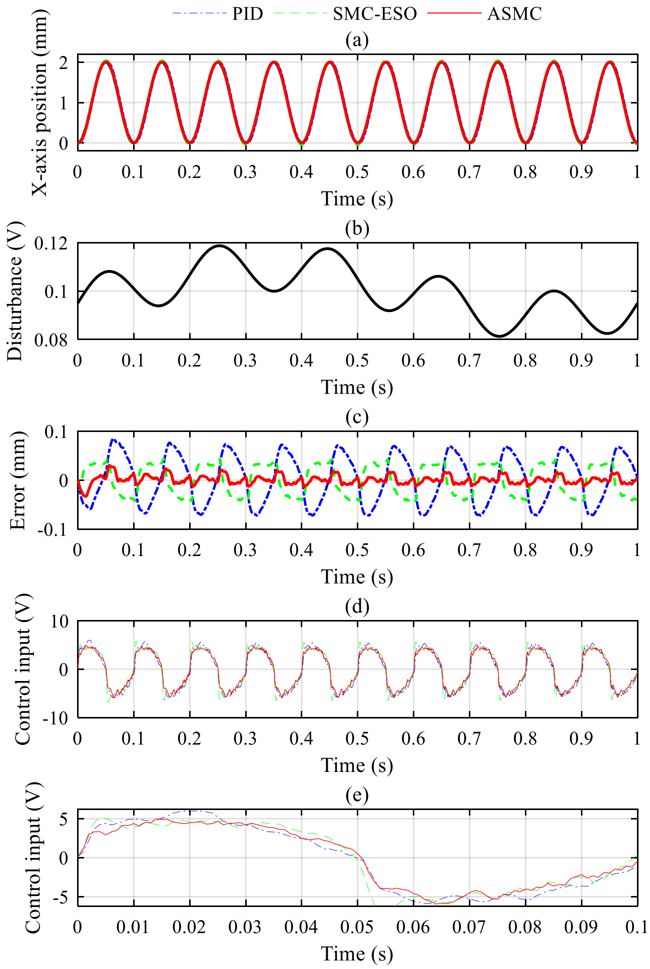

Fig. 10. Tracking results comparison of X-axis with the extreme disturbance.

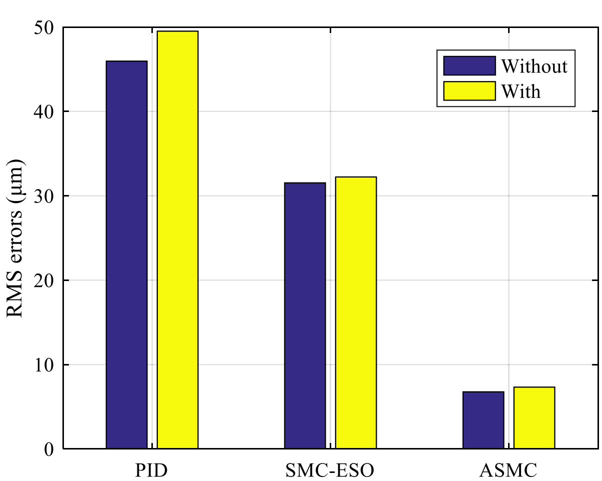

Fig. 11. Tracking errors comparison of with and without the extreme disturbance.

by linear PUMs. The model of the stage is derived with consideration of all uncertainties. Then, with a defined PID-type sliding mode function, the adjustable model-based control is designed. The high gain feedback term makes the system stable while the adaptive control term compensates for nonlinearities and uncertainties to improve the tracking performance. The control strategy is analyzed using a Lyapunov function for theoretical proof of its stability. The proposed control scheme

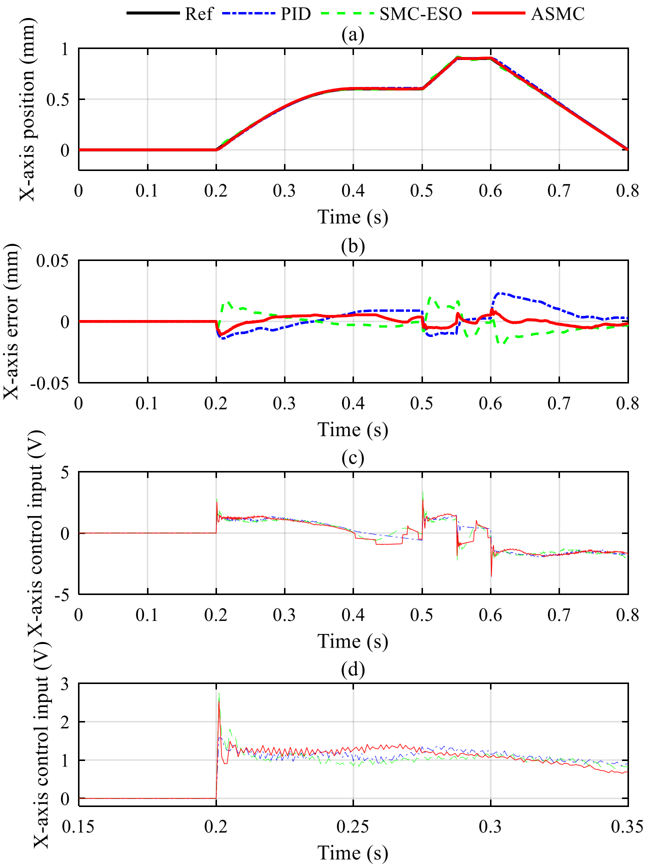

Fig. 12. Tracking results comparison of X-axis on specified motion.

Table 4
Specified motion tracking errors.

Errors (μm)	PID		SMC-ESO		ASMC	
	X	Y	X	Y	X	Y
μ_e	8.30	10.61	6.92	8.65	3.41	3.68
M_e	23.00	27.06	20.80	22.2	10.87	11.70
A_e	11.45		10.18		4.50	

is easy to implement with the easy tuning of controller parameters. Experiments are conducted on a 2-DOF stage to demonstrate the effectiveness of the proposed control scheme, which shows the proposed ASMC control scheme performs better than the other two methods.

CRediT authorship contribution statement

Min Ming: Methodology, Data curation, Writing - original draft. **Wenyu Liang:** Resources, Writing - review & editing. **Zhao Feng:** Software. **Jie Ling:** Investigation, Conceptualization. **Abdullah Al Mamun:** Supervision, Writing - review & editing. **Xiaohui Xiao:** Project administration.

Declaration of competing interest

The authors declare that they have no known competing financial interests or personal relationships that could have appeared to influence the work reported in this paper.

Acknowledgments

This work was supported by the China Postdoctoral Science Foundation under Grant No. 2018M642905, China Scholarship Council (CSC)

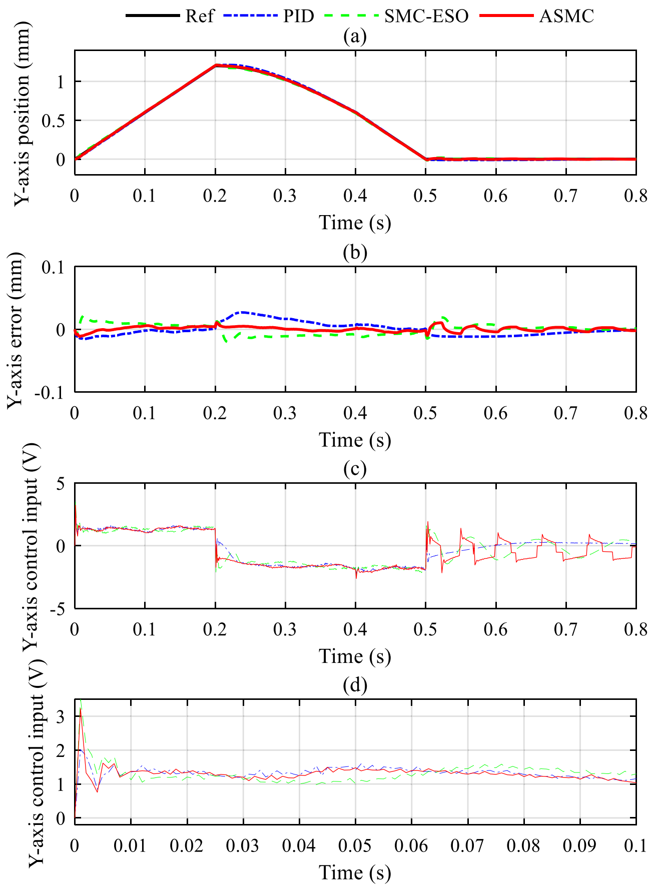

Fig. 13. Tracking results comparison of Y-axis on specified motion.

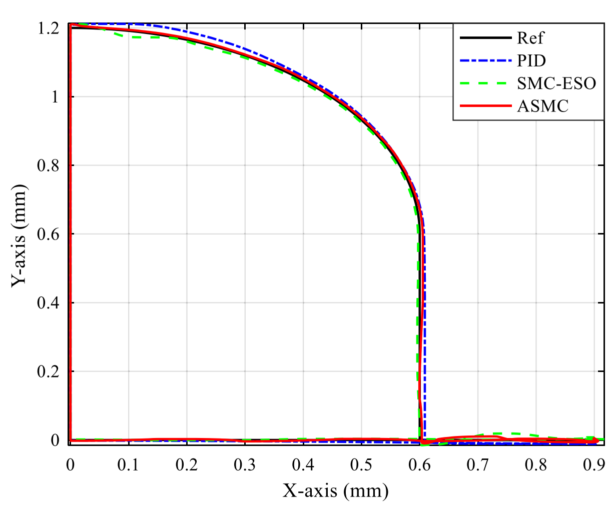

Fig. 14. Specified motion.

under Grant No. 201806270142 and Natural Science Foundation of China under Grant No. 51375349.

Appendix A. Supplementary data

Supplementary material related to this article can be found online at https://doi.org/10.1016/j.mechatronics.2021.102543.

References

[1] Habibullah H, Pota HR, Petersen IR. A novel control approach for high-precision positioning of a piezoelectric tube scanner. IEEE Trans Autom Sci Eng 2016;14(1):325–36.

[2] Ling J, Rakotondrabe M, Feng Z, Ming M, Xiao X. A robust resonant controller for high-speed scanning of nanopositioners: Design and implementation. IEEE Trans Control Syst Technol 2020;28(3):1116–23.

[3] Feng Z, Ling J, Ming M, Liang W, Tan KK, Xiao X. Signal-transformation-based repetitive control of spiral trajectory for piezoelectric nanopositioning stages. IEEE/ASME Trans Mechatronics 2020;28(3):1634–45.

[4] Al-Mamun A, Keikha E, Bhatia CS, Lee TH. Integral resonant control for suppression of resonance in piezoelectric micro-actuator used in precision servomechanism. Mechatronics 2013;23(1):1–9.

[5] Bhattarai U, Alouani AT. Flexible semi-automatic arm design for minimally invasive surgery. In: 2017 25th international conference on systems engineering. IEEE; 2017, p. 207–11.

[6] Simaan N, Yasin RM, Wang L. Medical technologies and challenges of robot-assisted minimally invasive intervention and diagnostics. Annu Rev Control Robot Auton Syst 2018;1:465–90.

[7] Kiong Tan K, Liang W, Le Pham P, Huang S, Wee Gan C, Yee Lim H. Design of a surgical device for office-based myringotomy and grommet insertion for patients with otitis media with effusion. J Med Devices 2014;8(3). (2014) 031001.

[8] Liang W, Ma J, Ng C, Ren Q, Huang S, Tan KK. Optimal and intelligent motion control scheme for an ultrasonic-motor-driven XY stage. Mechatronics 2019;59:127–39.

[9] Pan J, Cheung NC, Zou Y. High-precision control of LSRM based X–Y table for industrial applications. ISA Trans 2013;52(1):105–14.

[10] Ren B, Dai J, Zhong Q-C. UDE-based robust output feedback control with applications to a piezoelectric stage. IEEE Trans Ind Electron 2020;67(9):7819–28.

[11] Liu J, Vazquez S, Wu L, Marquez A, Gao H, Franquelo LG. Extended state observer-based sliding-mode control for three-phase power converters. IEEE Trans Ind Electron 2016;64(1):22–31.

[12] Cui M, Liu W, Liu H, Jiang H, Wang Z. Extended state observer-based adaptive sliding mode control of differential-driving mobile robot with uncertainties. Nonlinear Dynam 2016;83(1–2):667–83.

[13] Cui R, Chen L, Yang C, Chen M. Extended state observer-based integral sliding mode control for an underwater robot with unknown disturbances and uncertain nonlinearities. IEEE Trans Ind Electron 2017;64(8):6785–95.

[14] Wang H, Kong H, Man Z, Cao Z, Shen W, et al. Sliding mode control for steer-by-wire systems with AC motors in road vehicles. IEEE Trans Ind Electron 2013;61(3):1596–611.

[15] Xu Q. UDE-based adaptive sliding mode control of a piezoelectric nanopositioning stage. In: 2016 American control conference. IEEE; 2016, p. 673–8.

[16] Xu Q. Continuous integral terminal third-order sliding mode motion control for piezoelectric nanopositioning system. IEEE/ASME Trans Mechatronics 2017;22(4):1828–38.

[17] Ali SA, Langlois N. Sliding mode control for diesel engine air path subject to matched and unmatched disturbances using extended state observer. Math Probl Eng 2013;2013.

[18] Davis TA, Shin YC, Yao B. Adaptive robust control of circular machining contour error using global task coordinate frame. J Manuf Sci Eng 2015;137(1). (2015) 014501.

[19] Lau JY, Liang W, Tan KK. Motion control for piezoelectric-actuator-based surgical device using neural network and extended state observer. IEEE Trans Ind Electron 2019;67(1):402–12.

[20] Cheng L, Liu W, Hou Z-G, Yu J, Tan M. Neural-network-based nonlinear model predictive control for piezoelectric actuators. IEEE Trans Ind Electron 2015;62(12):7717–27.

[21] Li Y, Yang B, Zheng T, Li Y, Cui M, Peeta S. Extended-state-observer-based double-loop integral sliding-mode control of electronic throttle valve. IEEE Trans Intell Transp Syst 2015;16(5):2501–10.

[22] Yao J, Jiao Z, Ma D. RISE-based precision motion control of DC motors with continuous friction compensation. IEEE Trans Ind Electron 2014;61(12):7067–75.

[23] Liang W, Tan KK, Huang S, Pham LP, Lim HY, Gan CW. Control of a 2-DOF ultrasonic piezomotor stage for grommet insertion. Mechatronics 2013;23(8):1005–13.

[24] Huang S, Liang W, Tan KK. Intelligent friction compensation: A review. IEEE/ASME Trans Mechatronics 2019;24(4):1763–74.

[25] Escareno J-A, Rakotondrabe M, Habineza D. Backstepping-based robust-adaptive control of a nonlinear 2-DOF piezoactuator. Control Eng Pract 2015;41:57–71.

[26] Yao B, Tomizuka M. Adaptive robust control of SISO nonlinear systems in a semi-strict feedback form. Automatica 1997;33(5):893–900.

[27] Li C, Yao B, Wang Q. Modeling and synchronization control of a dual drive industrial gantry stage. IEEE/ASME Trans Mechatronics 2018;23(6):2940–51.

[28] Sun W, Liu Y, Gao H. Constrained sampled-data ARC for a class of cascaded nonlinear systems with applications to motor-servo systems. IEEE Trans Ind Inf 2018;15(2):766–76.

[29] Yao J, Deng W, Jiao Z. Rise-based adaptive control of hydraulic systems with asymptotic tracking. IEEE Trans Autom Sci Eng 2015;14(3):1524–31.
[30] Xian B, Dawson DM, de Queiroz MS, Chen J. A continuous asymptotic tracking control strategy for uncertain nonlinear systems. IEEE Trans Automat Control 2004;49(7):1206–11.
[31] Wang S, Na J, Ren X. RISE-based asymptotic prescribed performance tracking control of nonlinear servo mechanisms. IEEE Trans Syst Man Cybern A 2017;48(12):2359–70.
[32] Li Y, Xu Q. Adaptive sliding mode control with perturbation estimation and PID sliding surface for motion tracking of a piezo-driven micromanipulator. IEEE Trans Control Syst Technol 2009;18(4):798–810.
[33] Gao P, Zhang G, Ouyang H, Mei L. A sliding mode control with nonlinear fractional order PID sliding surface for the speed operation of surface-mounted PMSM drives based on an extended state observer. Math Probl Eng 2019;2019.
[34] Xie M, Yu S, Lin H, Ma J, Wu H. Improved sliding mode control with time delay estimation for motion tracking of cell puncture mechanism. IEEE Trans Circuits Syst I Regul Pap 2020;67(9):3199–210.
[35] Rakotondrabe M. Modeling and robust h∞ control of a nonlinear and oscillating 2-DOF multimorph cantilevered piezoelectric actuator. In: Smart materials-based actuators at the micro/nano-scale. Springer; 2013, p. 61–88.

Min Ming received the B.S. degrees in Mechanical Engineering from School of Power and Mechanical Engineering, Wuhan University, Wuhan, China in 2016. She is currently pursuing the Ph.D. degree in Mechanical Engineering at Wuhan University, Wuhan, China. She is now as a visiting Ph.D. student at the Department of Electrical and Computer Engineering, National University of Singapore. Her research interest covers hysteresis compensation, precision motion control, and nano-positioner.

Wenyu Liang received the B.Eng. and M.Eng. degrees in mechanical engineering from the China Agricultural University, Beijing, China, in 2008 and 2010, respectively, and the Ph.D. degree in electrical and computer engineering from the National University of Singapore, Singapore, in 2014. He is currently a Scientist with the Institute for Inforcomm Research, A*STAR, Singapore and also an Adjunct Assistant Professor with the Department of Electrical and Computer Engineering, National University of Singapore. His research interests mainly include robotics, mechatronics and automation, precision motion control and force control with applications in medical and industrial technology.

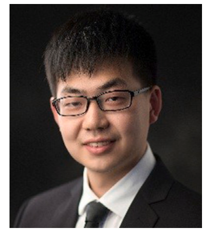

Zhao Feng received the B.S. degrees in Mechanical Engineering from School of Power and Mechanical Engineering, Wuhan University, Wuhan, China in 2014. From 2019 to 2020, he was as a visiting Ph.D. student at the Department of Electrical and Computer Engineering, National University of Singapore. He is currently pursuing the Ph.D. degree in Mechanical Engineering at Wuhan University, Wuhan, China. His research interests include vibration control, iterative learning control, nanopositioning and robotics.

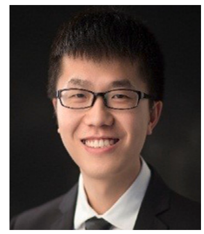

Jie Ling received his B.S. and Ph.D. degrees in Mechanical Engineering from School of Power and Mechanical Engineering, Wuhan University, China, in 2012 and 2018, respectively. He was a joint Ph.D. student with Department of Automatic Control and Micro-Mechatronic Systems, FEMTO-st Institute, France in 2017. From 2019 to 2020, he is a joint Postdoc Researcher with Department of Biomedical Engineering, National University of Singapore, Singapore. Since 2018, he has been a Postdoctoral Researcher with Department of Mechanical Engineering, Wuhan University, Wuhan, China. His research interests include mechanical design and precision motion control of nanopositioning stages and micromanipulation robots.

Abdullah Al Mamun is an associate professor in the department of Electrical and Computer Engineering of the National University of Singapore. He obtained Bachelor of Technology (Honours) degree from Indian Institute of Technology (IIT), Kharagpur, and Ph.D. from National University of Singapore. His research interests include mechatronics, precision control systems, and intelligent control of motors and drives. He is a senior member of IEEE.

Xiaohui Xiao received the B.S. and M.S. degrees in Mechanical Engineering from Wuhan University, Wuhan, China, in 1991 and 1998, respectively, and the Ph.D. degree in mechanical engineering from Huazhong University of Science and Technology, Wuhan, China, in 2005. She joined the Wuhan University, Wuhan, China, in 1998, where she is currently a Full Professor with the Mechanical Engineering Department, School of Power and Mechanical Engineering. Her current research interests include mobile robotics, high-precision positioning control, and signal processing.